Anisotropic magnetic and transport properties of orthorhombic $Al_{13}Co_4$

J. Dolinšek,[1] M. Komelj,[1] P. Jeglič,[1] S. Vrtnik,[1] D. Stanić,[2] P. Popčević,[2] J. Ivkov,[2] A. Smontara,[2] Z. Jagličić,[3] P. Gille,[4] and Yu. Grin[5]

[1]*J. Stefan Institute, University of Ljubljana, Jamova 39, SI-1000 Ljubljana, Slovenia*

[2]*Institute of Physics, Laboratory for the Study of Transport Problems, Bijenička 46, P.O. Box 304, HR-10001 Zagreb, Croatia*

[3]*Institute of Mathematics, Physics, and Mechanics, University of Ljubljana, Jadranska 19, SI-1000 Ljubljana, Slovenia*

[4]*Department of Earth and Environmental Sciences, Crystallography Section, Ludwig-Maximilians-Universität München, Theresienstrasse 41, D-80333 München, Germany*

[5]*Max-Planck-Institut für Chemische Physik fester Stoffe, Nöthnitzer Str. 40, D-01187 Dresden, Germany*

(Received 17 December 2008; revised manuscript received 23 March 2009; published 6 May 2009)

We have investigated anisotropic physical properties (magnetic susceptibility, electrical resistivity, thermoelectric power, Hall coefficient, and thermal conductivity) of the *o*-$Al_{13}Co_4$, an orthorhombic approximant to the decagonal phase. The crystallographic-direction-dependent measurements were performed along the *a*, *b*, and *c* directions of the orthorhombic unit cell, where (*b*,*c*) atomic planes are stacked along the perpendicular *a* direction. Magnetic susceptibility is predominantly determined by the Pauli-spin paramagnetism of conduction electrons. The in-plane magnetism is stronger than that along the stacking *a* direction. Anisotropic electrical and thermal conductivities are the highest along the stacking *a* direction. The anisotropic thermoelectric power changes sign with the crystallographic direction and so does the anisotropic Hall coefficient which changes from negative electronlike to positive holelike for different combinations of the electric current and magnetic-field directions. The investigated anisotropic electrical and thermal transport coefficients were reproduced theoretically by *ab initio* calculation using Boltzmann transport theory and the calculated anisotropic Fermi surface. The calculations were performed for two structural models of the *o*-$Al_{13}Co_4$ phase, where the more recent model gave better agreement, though still qualitative only, to the experiments.

DOI: 10.1103/PhysRevB.79.184201 PACS number(s): 61.44.Br, 71.23.Ft

I. INTRODUCTION

Decagonal quasicrystals (*d*-QCs) can be structurally viewed as a periodic stack of quasiperiodic atomic planes so that *d*-QCs are two-dimensional (2D) quasicrystals, whereas they are periodic crystals in a direction perpendicular to the quasiperiodic planes. A consequence of the structural anisotropy are anisotropic electrical and thermal transport properties [electrical resistivity ρ,[1–3] thermoelectric power S,[4] Hall coefficient R_H,[5,6] thermal conductivity κ,[7,8] and optical conductivity $\sigma(\omega)$ [9]], when measured along the quasiperiodic (Q) and periodic (P) crystallographic directions. A striking example of the anisotropic nature of *d*-QCs is their electrical resistivity, which shows positive temperature coefficient (PTC) at metallic values along the P direction (e.g., $\rho_P^{300\ \mathrm{K}} \approx 40\ \mu\Omega$ cm in *d*-Al-Cu-Co and *d*-Al-Ni-Co),[2] whereas the resistivity in the quasiperiodic plane is considerably larger (e.g., $\rho_Q^{300\ \mathrm{K}} \approx 330\ \mu\Omega$ cm)[2] and exhibits a negative temperature coefficient (NTC) and sometimes also a maximum somewhere below room temperature (RT) or a leveling off upon $T \to 0$. The anisotropy of the Hall coefficient R_H is another intriguing feature of *d*-QCs being positive holelike ($R_H > 0$) for the magnetic field lying in the quasiperiodic plane, whereas it changes sign to negative ($R_H < 0$) for the field along the periodic direction thus becoming electronlike. This R_H anisotropy was reported for the *d*-Al-Ni-Co, *d*-Al-Cu-Co, and *d*-Al-Si-Cu-Co and is considered to be a universal feature of *d*-QCs.[5,6]

The degree of anisotropy of the transport coefficients is related to the structural details of a particular decagonal phase, depending on the number of quasiperiodic layers in one periodic unit.[10,11] The most anisotropic case are the phases with just two layers, realized in *d*-Al-Ni-Co and *d*-Al-Cu-Co, where the periodicity length along the periodic axis is about 0.4 nm and the resistivity ratio at RT amounts typically $\rho_Q/\rho_P \approx 6-10$.[1–3] Other *d* phases contain more quasiperiodic layers in a periodic unit and show smaller anisotropies. In *d*-Al-Co, *d*-Al-Ni, and *d*-Al-Si-Cu-Co there are four quasiperiodic layers with periodicity of about 0.8 nm and the RT anisotropy is $\rho_Q/\rho_P \approx 2-4$.[4] *d*-Al-Mn, *d*-Al-Cr, and *d*-Al-Pd-Mn phases contain six layers with periodicity of about 1.2 nm and the anisotropy amounts $\rho_Q/\rho_P \approx 1.2-1.4$, whereas *d*-Al-Pd and *d*-Al-Cu-Fe phases with eight layers in a periodicity length of 1.6 nm are close to isotropic. While the origin of the anisotropic electron-transport coefficients is the anisotropic Fermi surface, the anisotropy of which originates from the specific stacked-layer crystal structure of the *d*-QCs phases and the chemical decoration of the lattice, the lack of translational periodicity within the quasiperiodic planes prevents any quantitative theoretical analysis of this phenomenon. The problem can be overcome by considering approximant phases to the decagonal phase, for which—being periodic solids in three dimensions—theoretical simulations are straightforward to perform. Approximant phases are characterized by large unit cells which periodically repeat in space with the atomic decoration closely resembling that of *d*-QCs. Atomic layers are again stacked periodically and the periodicity lengths along the stacking direction are almost identical to those along the periodic direction of *d*-QCs. Moreover, atomic planes of approximants and *d*-QCs show locally similar patterns so that their structures on the scale of near-neighbor

atoms closely resemble each other. Decagonal approximants thus offer valid comparison to the *d*-QCs.

Recently, the anisotropic magnetic and transport properties (magnetic susceptibility, electrical resistivity, thermoelectric power, Hall coefficient, and thermal conductivity), measured along three orthogonal crystallographic directions, were reported for the $Al_{76}Co_{22}Ni_2$ compound,[12] known also as the Y phase of Al-Ni-Co (hereafter abbreviated as Y-Al-Ni-Co). Y-Al-Ni-Co belongs to the $Al_{13}TM_4$ (TM =transition metal) group of complex metallic compounds and is a monoclinic approximant to the decagonal phase with two atomic layers within one periodic unit of ≈0.4 nm along the stacking direction and a relatively small unit cell comprising 32 atoms. The investigated transport properties of the Y-Al-Ni-Co were found typical metallic with PTC resistivity in all crystallographic directions, showing pronounced anisotropy, where the crystal is most conducting for both the electricity and heat along the stacking direction (corresponding to the periodic direction in *d*-QCs). Anisotropic magnetic susceptibility of conduction electrons was found paramagnetic for the field lying within the atomic planes and diamagnetic for the field along the stacking direction. Anisotropic magnetic and transport properties were also reported for the $Al_4(Cr,Fe)$ complex metallic compound with the composition $Al_{80}Cr_{15}Fe_5$.[13,14] This phase belongs to the group of orthorhombic Al_4TM phases first described by Deng *et al.*,[15] which are approximants to the decagonal phase with six atomic layers in a periodic unit of 1.25 nm and 306 atoms in the giant unit cell. The measurements showed that the in-plane electrical resistivity of this compound exhibits nonmetallic behavior with NTC and a maximum in $\rho(T)$, whereas the resistivity along the stacking direction shows PTC.

In this paper we report a study of the anisotropic physical properties (magnetic susceptibility, electrical resistivity, thermoelectric power, Hall coefficient, and thermal conductivity) of the orthorhombic o-$Al_{13}Co_4$ complex metallic compound, belonging to the $Al_{13}TM_4$ group of decagonal approximants with four atomic layers within one periodic unit of ≈0.8 nm along the stacking direction and a unit cell comprising 102 atoms. This study complements our previous work on the anisotropic physical properties of the decagonal approximant phases, the aforementioned Y-Al-Ni-Co with two atomic layers within one periodic unit of ≈0.4 nm and 32 atoms in the relatively small unit cell and the $Al_4(Cr,Fe)$ with six atomic layers within one periodic unit of ≈1.25 nm and 306 atoms in the large unit cell. The o-$Al_{13}Co_4$ phase with four atomic layers and 102 atoms in the unit cell is thus intermediate to the other two approximant phases regarding the number of layers in one periodic unit and the size of the unit cell so that a comparison of the three phases can be used to consider how do the anisotropic physical properties of the decagonal approximant phases evolve with increasing structural complexity and the unit-cell size.

II. STRUCTURAL CONSIDERATIONS AND SAMPLE PREPARATION

The orthorhombic o-$Al_{13}Co_4$ phase[16] belongs to the $Al_{13}TM_4$ group of decagonal approximants. Other members of this class are monoclinic m-$Al_{13}Co_4$,[17] monoclinic $Al_{13}Fe_4$,[18] monoclinic $Al_{13-x}(Co_{1-y}Ni_y)_4$ (the Y phase),[19] monoclinic $Al_{13}Os_4$,[20] $Al_{13}Ru_4$ (isotypical to $Al_{13}Fe_4$),[21] and $Al_{13}Rh_4$ (also isotypical to $Al_{13}Fe_4$).[22] According to the structural model by Grin *et al.*,[16] lattice parameters of the o-$Al_{13}Co_4$ orthorhombic unit cell (space group $Pmn2_1$ and Pearson symbol $oP102$) are a=0.8158 nm, b=1.2342 nm, and c=1.4452 nm with 102 atoms in the unit cell. The structure corresponds to a four-layer stacking along [100],[16,19] with flat layers at $x=0$ and $x=\frac{1}{2}$ and two symmetrically equivalent puckered layers at $x=\frac{1}{4}$ and $\frac{3}{4}$, giving ≈0.8 nm period along [100]. Based on a recent more precise crystal structure determination, Grin *et al.*[23] have reported that the o-$Al_{13}Co_4$ structure can be described alternatively as a cage compound, where linear Co-Al-Co species (called the "*Würstchen*") extended along [100] are embedded within atomic cages, where the chemical bonding within the Co-Al-Co unit and between the unit and the remaining framework are different.

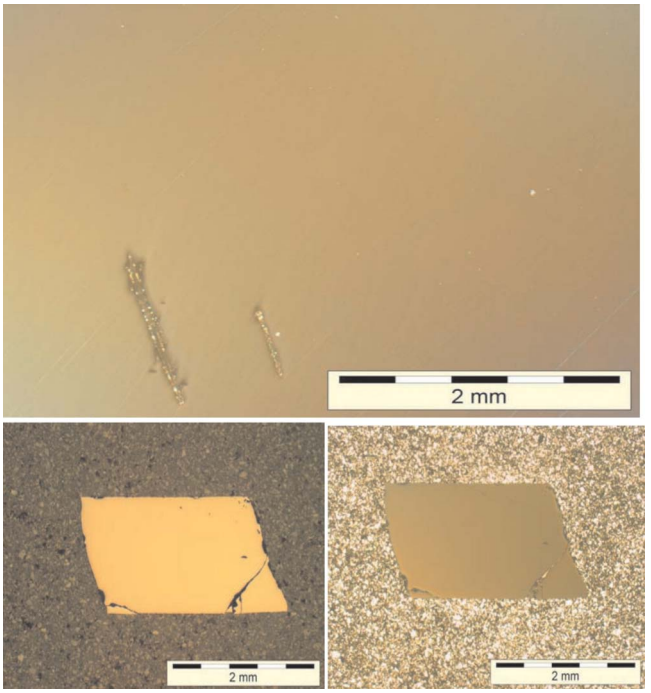

FIG. 1. (Color online) Microstructure of the large area of an as-grown ingot of o-$Al_{13}Co_4$: optical investigations in nonpolarized (bottom left) and polarized (bottom right) light show the absence of grain boundaries, thus confirming single-crystalline character of the material.

The o-$Al_{13}Co_4$ single crystal used in our study was grown by the Czochralski technique (the details are described elsewhere[24]) and its structure matched well to the orthorhombic unit cell of the Grin *et al.*[16] model. Metallographic analysis (Fig. 1) revealed that the whole ingot was a single crystal, free of secondary phases and grain boundaries. In order to perform crystallographic-direction-dependent studies, we have cut from the ingot three bar-shaped specimens of dimensions $2\times2\times7$ mm^3, with their long axes along three orthogonal directions. The long axis of the first sample was along the [100] stacking direction (designated in the follow-

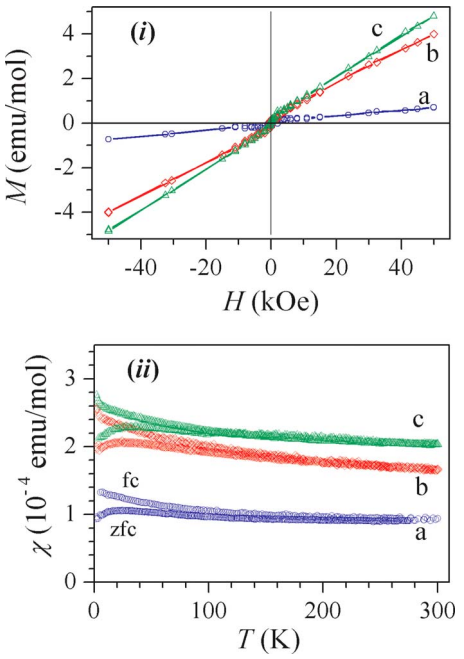

FIG. 2. (Color online) (i) Magnetization M of o-$Al_{13}Co_4$ as a function of the magnetic field H at $T=5$ K with the field oriented along three orthogonal crystallographic directions a, b, and c. (ii) Temperature-dependent magnetic susceptibility $\chi=M/H$ in the field $H=1$ kOe applied along the three crystallographic directions. Both zfc and fc runs are shown.

ing as a), which corresponds to the pseudotenfold axis of the o-$Al_{13}Co_4$ structure and is equivalent to the periodic (tenfold) direction in the related d-QCs. The (b,c) orthorhombic plane corresponds to the quasiperiodic plane in the d-QCs and the second sample was cut with its long axis along the [010] (b) direction, and the third one along the [001] (c) direction. For each sample, the orientation of the other two crystallographic directions was also known. The so-prepared specimens enabled us to determine the anisotropic physical properties of the o-$Al_{13}Co_4$ phase along the three principal orthorhombic directions of the unit cell.

III. EXPERIMENTAL RESULTS

A. Magnetization and magnetic susceptibility

The magnetization as a function of the magnetic field $M(H)$ and the temperature-dependent magnetic susceptibility $\chi(T)$ were investigated in the temperature interval between 300 and 2 K using a Quantum Design superconducting quantum interference device magnetometer equipped with a 50 kOe magnet. In the orientation-dependent measurements, the magnetic field was directed along the long axis of each sample, thus along the a, b, and c crystallographic directions. The $M(H)$ curves at $T=5$ K are displayed in Fig. 2(i). For all three directions, the $M(H)$ dependence is linear and positive paramagnetic in the whole investigated field range up to 50 kOe, except in the close vicinity of $H=0$, where a curvature typical of a small ferromagnetic (FM) component in the magnetization is observed. The $M(H)$ curves show anisotropy in the slopes in the following order: $(\partial M/\partial H)_a \ll (\partial M/\partial H)_b < (\partial M/\partial H)_c$. The anisotropy between the two in-plane directions b and c is small, whereas the anisotropy between the in-plane directions and the stacking direction a is considerably larger.

The experimental $M(H)$ curves were reproduced theoretically by the expression

$$M = M_0 L(\mu H/k_B T) + kH. \quad (1)$$

The first term describes the FM contribution, where M_0 is the saturated magnetization and $L(x)=\coth(x)-1/x$ is the Langevin function that is a limit of the Brillouin function for large magnetic moments μ (or total angular momentum J, related to the magnetic moment by $\mu=g\mu_B J$, where μ_B is the Bohr magneton and g is the Landé factor, taken as 2 in our analysis). This function reproduces well the $M(H)$ dependence of the FM component but with an unphysically large magnetic moment μ so that its validity is merely to enable extraction of the second term, kH, from the total magnetization. Here k represents the terms in the susceptibility $\chi=M/H$ that are linear in the magnetic field (the Larmor core diamagnetic susceptibility estimated from literature tables[25] to amount $\chi_{\text{Larmor}}=-7.4\times10^{-5}$ emu/mol and the susceptibility of the conduction electrons—the Pauli-spin paramagnetic contribution and the Landau orbital diamagnetic contribution). The positive linear $M(H)$ dependence for all three directions up to the highest investigated field suggests predominant role of the Pauli paramagnetism.

The fits with Eq. (1) are shown in Fig. 3, and the fit parameters are given in Table I. The k values are in the range 10^{-5} emu/mol, thus of the same order as the (negative) Larmor susceptibility, as expected for the conduction-electron susceptibility. From Fig. 3 it is evident that the FM contribution saturates already in a low field of about $H\approx3$ kOe, a value typical for a FM-type magnetization. The microscopic origin of the small FM component is not clear but very similar FM contributions were reported also for the Y-Al-Ni-Co approximant[12] and the related d-$Al_{72}Ni_{12}Co_{16}$ (Ref. 26) and d-$Al_{70}Ni_{15}Co_{15}$ (Ref. 27) quasicrystals, where it was suggested that they originated from the Co- and/or Ni-rich regions in the samples. Similar consideration of the Co-rich regions could apply also to our o-$Al_{13}Co_4$. Here it is important to note that structural considerations of the Grin *et al.*[16] model do not suggest any Co-rich domains within the perfect o-$Al_{13}Co_4$ phase so that the experimentally detected FM contributions should be associated with defects in the crystal, perhaps with the FM impurities in ppm concentrations in the starting materials. Using the M_0 values from Table I and assuming the Co^{2+} electronic state, we can estimate the fraction of magnetic Co atoms within the FM clusters relative to the total number of Co atoms in the samples. In a solid environment, the angular momentum J of a Co^{2+} ion roughly equals its spin quantum number $S=\frac{3}{2}$ so that the maximum moment per Co^{2+} amounts $M_{0,\max}=g\mu_B J=3\mu_B$, whereas it amounts $M_{0,\max}=12\mu_B$ per one $Al_{13}Co_4$ molecule. Using the M_0 values from Table I (by recalculating them from the emu/mol units into μ_B per $Al_{13}Co_4$ molecule), we obtain the FM Co fraction $f=M_0/M_{0,\max}=1.7\times10^{-6}$ for the a direction, $f=4.0\times10^{-6}$ for the b direction, and $f=3.7\times10^{-6}$ for the c

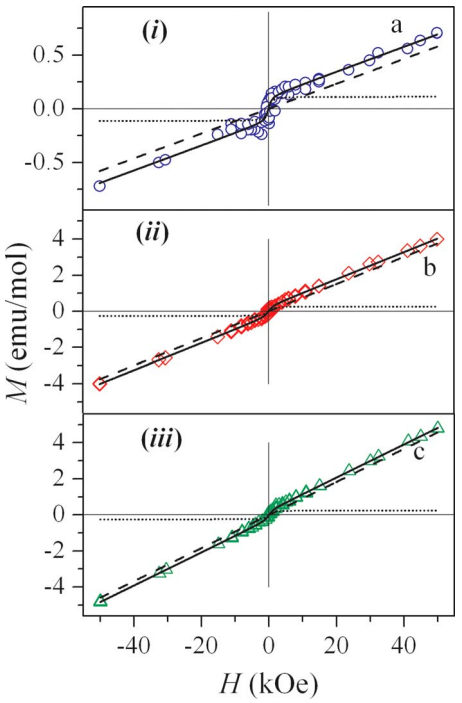

FIG. 3. (Color online) Analysis of the $M(H)$ curves from Fig. 2 [panel (i): a direction, panel (ii): b direction, and panel (iii): c direction]. Solid curves are fits with Eq. (1), dashed lines represent the term of the magnetization linear in the magnetic field, kH, (the Larmor core contribution and the contribution due to the conduction electrons) and dotted curves are the FM contribution. The fit parameters are given in Table I.

direction (or $\bar{f}=3.1\times10^{-6}$, when averaged over the three directions). These values, of a few ppm, show that the volume of the FM domains is very small as compared to the total volume of the samples so that their origin from the FM impurities in the starting materials seems to be preferable.

The temperature-dependent magnetic susceptibility $\chi(T)$ along the three crystallographic directions a, b, and c, measured in a field of 1 kOe, is displayed in Fig. 2(ii). For each direction, both zero-field-cooled (zfc) and field-cooled (fc) temperature runs were performed. The existence of the FM component in the susceptibility is manifested in the zfc-fc susceptibility splitting, observed below about 100 K. Due to the presence of the zfc-fc splitting, which demonstrates remanence of the spins within the FM clusters, the temperature dependence of the susceptibility is not straightforward to analyze and we skip it here. Regarding the anisotropy of the susceptibility, it appears in the order $\chi_a<\chi_b<\chi_c$, in agreement with the anisotropy determined from the $M(H)$ relation in Fig. 2(i).

TABLE I. Parameters of the $M(H)$ fits (solid curves in Fig. 3) using Eq. (1). Parameter f denotes the fraction of magnetic Co atoms within the FM clusters relative to the total number of Co atoms in the samples.

Crystallographic direction	M_0 (emu/mol)	μ (μ_B)	f	k (emu/mol)
a	0.114	189	1.7×10^{-6}	1.16×10^{-5}
b	0.267	138	4.0×10^{-6}	7.50×10^{-5}
c	0.247	160	3.7×10^{-6}	9.16×10^{-5}

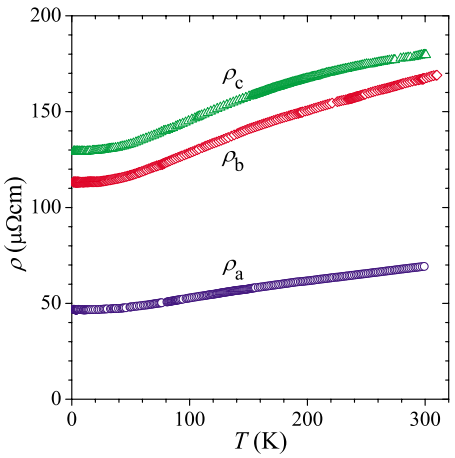

FIG. 4. (Color online) Temperature-dependent electrical resistivity of o-$Al_{13}Co_4$ along three orthogonal crystallographic directions a, b, and c.

Magnetic properties of the o-$Al_{13}Co_4$ thus show considerable anisotropy for different crystallographic directions. The in-plane anisotropy of the magnetization and the susceptibility is relatively weak, whereas the anisotropy between the in-plane directions and the stacking a direction is stronger. The linear paramagnetic $M(H)$ relation suggests that the susceptibility is predominantly determined by the Pauli-spin paramagnetism of conduction electrons. This anisotropy should have its microscopic origin in the anisotropy of the Fermi surface.

B. Electrical resistivity

Electrical resistivity was measured between 300 and 2 K using the standard four-terminal technique. The $\rho(T)$ data along the three crystallographic directions are displayed in Fig. 4. The resistivity is the lowest along the stacking a direction perpendicular to the atomic planes, where its RT value amounts $\rho_a^{300\ \mathrm{K}}=69\ \mu\Omega$ cm and the residual resistivity is $\rho_a^{2\ \mathrm{K}}=47\ \mu\Omega$ cm. The two in-plane resistivities are higher, amounting $\rho_b^{300\ \mathrm{K}}=169\ \mu\Omega$ cm and $\rho_b^{2\ \mathrm{K}}=113\ \mu\Omega$ cm for the b direction and $\rho_c^{300\ \mathrm{K}}=180\ \mu\Omega$ cm and $\rho_c^{2\ \mathrm{K}}=129\ \mu\Omega$ cm for the c direction. The anisotropy of the two in-plane resistivities is small, amounting at RT to $\rho_c^{300\ \mathrm{K}}/\rho_b^{300\ \mathrm{K}}=1.07$, whereas the anisotropy to the stacking direction is considerably larger, $\rho_c^{300\ \mathrm{K}}/\rho_a^{300\ \mathrm{K}}=2.6$ and $\rho_b^{300\ \mathrm{K}}/\rho_a^{300\ \mathrm{K}}=2.5$. The anisotropic resistivities thus appear in the order $\rho_a<\rho_b<\rho_c$ (even the inequality $\rho_a\ll\rho_b<\rho_c$ may be considered to hold), which is the same order as that of the anisotropic magnetic susceptibility. This anisotropy will be further discussed in the following by considering the anisotropic Fermi surface of the o-$Al_{13}Co_4$ phase. The PTC of the resistivity along all three crystallographic directions demonstrates predominant role of the electron-phonon-scattering mechanism.

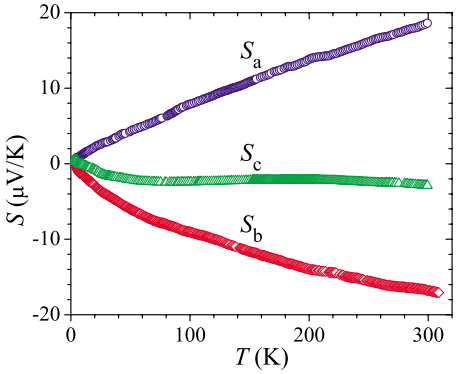

FIG. 5. (Color online) Temperature-dependent thermoelectric power (the Seebeck coefficient S) of o-$Al_{13}Co_4$ along three orthogonal crystallographic directions a, b, and c.

C. Thermoelectric power

The thermoelectric power (the Seebeck coefficient S) was measured between 300 and 2 K by using a standard temperature-gradient technique. The thermopower data, measured along the three crystallographic directions a, b, and c, are displayed in Fig. 5. The thermopower appears in the order $S_a > S_c > S_b$ and shows astonishing anisotropy: it is positive along the stacking a direction with the RT value $S_a^{300\ \mathrm{K}} = 18.6\ \mu\mathrm{V/K}$, it becomes almost symmetrically negative for the in-plane b direction with $S_b^{300\ \mathrm{K}} = -17.1\ \mu\mathrm{V/K}$ and is close to zero for the second in-plane c direction, amounting $S_c^{300\ \mathrm{K}} = -2.9\ \mu\mathrm{V/K}$. While S_a and S_b exhibit relatively strong linearlike temperature dependence (a small change of slope at about 50 K may be noticed, a feature that is often associated with electron-phonon effects), S_c shows almost no temperature dependence in the investigated temperature range. The observed anisotropy of the thermopower, ranging between positive and negative values, demonstrates that the Fermi surface is highly anisotropic, consisting of electronlike and holelike parts, which may compensate each other for some crystallographic direction to yield a thermopower close to zero. Moreover, the anisotropy of the phonon spectrum may contribute to the anisotropic thermopower via the anisotropic electron-phonon interaction as well (the importance of phonons in the electron transport of o-$Al_{13}Co_4$ is manifested in the PTC electrical resistivity of Fig. 4). This remarkable anisotropy of the thermopower will be discussed further in the following by considering the anisotropic Fermi surface of the o-$Al_{13}Co_4$.

It should be remarked that the anisotropic thermopower of o-$Al_{13}Co_4$ shown in Fig. 5 changes sign monotonously with the direction of the temperature gradient relative to the crystallographic axes in the whole investigated temperature range between RT and 2 K, thus enabling to sense the direction of the thermal source relative to the o-$Al_{13}Co_4$ crystallographic axes, a feature that may serve for the application of this material to the orientation-sensing thermoelectric devices.

D. Hall coefficient

The Hall-effect measurements were performed by the five-point method using standard ac technique in magnetic fields up to 10 kOe. The current through the samples was in the range 10–50 mA. The measurements were performed in the temperature interval from 90 to 390 K. The temperature-dependent Hall coefficient $R_H = E_y/j_x B_z$ is displayed in Fig. 6. In order to determine the anisotropy of R_H, three sets of experiments were performed with the current along the long axis of each sample (thus along a, b, and c, respectively), whereas the magnetic field was directed along each of the other two orthogonal crystallographic directions, making six experiments altogether. For all combinations of directions, the R_H values are typical metallic in the range 10^{-10} $\mathrm{m^3\ C^{-1}}$ (with the experimental uncertainty of $\pm 0.1 \times 10^{-10}$ $\mathrm{m^3\ C^{-1}}$). R_H exhibit pronounced anisotropy with the following regularity. The six R_H sets of data form three groups of two practically identical R_H curves, where the magnetic field in a given crystallographic direction yields the same R_H for the current along the other two crystallographic directions in the perpendicular plane. Thus, identical Hall coefficients are obtained for combinations $E_b/j_c B_a = E_c/j_b B_a = R_H^a$ (where the additional superscript on the Hall coefficient denotes the direction of the magnetic field), amounting $R_H^a(300\ \mathrm{K}) = -6.5 \times 10^{-10}$ $\mathrm{m^3\ C^{-1}}$, $E_a/j_c B_b = E_c/j_a B_b = R_H^b$ with $R_H^b(300\ \mathrm{K}) = 3.5 \times 10^{-10}$ $\mathrm{m^3\ C^{-1}}$ and $E_b/j_a B_c = E_a/j_b B_c = R_H^c$ with $R_H^c(300\ \mathrm{K}) = -0.6 \times 10^{-10}$ $\mathrm{m^3\ C^{-1}}$. The anisotropic R_H values are also collected in Table II. R_H^b and R_H^c are practically temperature independent within the investigated temperature

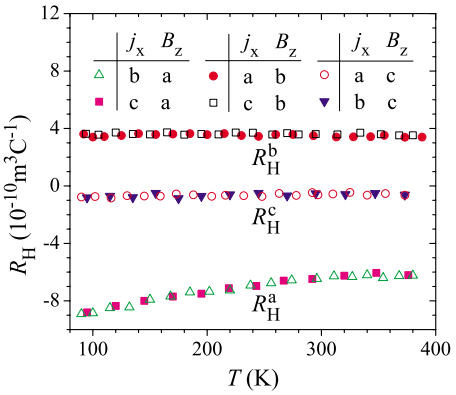

FIG. 6. (Color online) Anisotropic temperature-dependent Hall coefficient $R_H = E_y/j_x B_z$ of o-$Al_{13}Co_4$ for different combinations of directions of the current j_x and magnetic field B_z (given in the legend). The superscript a, b, or c on R_H denotes the direction of the magnetic field.

TABLE II. Anisotropic Hall coefficient $R_H = E_y/j_x B_z$ of the o-$Al_{13}Co_4$ for various directions of the current and field.

Current direction (j_x)	Field direction (B_z)	R_H(300 K) (10^{-10} $\mathrm{m^3\ C^{-1}}$)
a	b	3.5
	c	−0.6
b	a	−6.5
	c	−0.5
c	a	−6.5
	b	3.5

range, whereas R_H^a shows moderate temperature dependence that tends to disappear at higher temperatures.

The observed R_H anisotropy reflects complicated structure of the Fermi surface. The negative $R_H^a<0$ is electronlike for the magnetic field along the stacking a direction, whereas the positive $R_H^b>0$ behaves holelike for the field along the in-plane b direction. For the field along the second in-plane direction c, $R_H^c\approx 0$ suggests that electronlike and holelike contributions are of comparable importance. This orientation dependent mixed electronlike and holelike behavior of the anisotropic Hall coefficient is analogous to the anisotropy of the thermopower, presented in Fig. 5, which also changes sign with the crystallographic direction. In both cases there is no simple explanation of this dual behavior, which requires knowledge of the details of the anisotropic Fermi surface pertinent to the o-$Al_{13}Co_4$ phase and will be discussed in the following. Here it is worth mentioning that the anisotropic Hall coefficient of the d-Al-Ni-Co-type QCs shows similar duality, being also holelike $R_H>0$ for the field lying in the quasiperiodic plane and electronlike $R_H<0$ for the field along the periodic direction.[5,6] This duality is proposed to be a universal feature of d-QCs.

E. Thermal conductivity

Thermal conductivity κ of o-$Al_{13}Co_4$ was measured along the a, b, and c directions using an absolute steady-state heat-flow method. The thermal flux through the samples was generated by a 1 kΩ RuO_2 chip-resistor, glued to one end of the sample, while the other end was attached to a copper heat sink. The temperature gradient across the sample was monitored by a chromel-constantan differential thermocouple. The phononic contribution $\kappa_{ph}=\kappa-\kappa_{el}$ was estimated by subtracting the electronic contribution κ_{el} from the total conductivity κ using the Wiedemann-Franz law, $\kappa_{el}=\pi^2k_B^2T\sigma(T)/3e^2$ and the measured electrical conductivity data $\sigma(T)=\rho^{-1}(T)$ from Fig. 4. The total thermal conductivity κ along the three crystallographic directions is displayed in the upper panel of Fig. 7 and the electronic contribution κ_{el} is shown by solid curves. At 300 K, we get the following anisotropy: $\kappa^a=12.5$ W/mK, $\kappa_{el}^a=10.2$ W/mK with their ratio $(\kappa_{el}^a/\kappa^a)_{300\ K}=0.82$, $\kappa^b=6.1$ W/mK, $\kappa_{el}^b=4.4$ W/mK with $(\kappa_{el}^b/\kappa^b)_{300\ K}=0.72$, and $\kappa^c=6.2$ W/mK, $\kappa_{el}^c=4.1$ W/mK with $(\kappa_{el}^c/\kappa^c)_{300\ K}=0.66$. Electrons (and holes) are thus majority heat carriers at RT for all three directions. The anisotropic thermal conductivities appear in the order $\kappa^a>\kappa^b\approx\kappa^c$ and the same order applies to the electronic parts $\kappa_{el}^a>\kappa_{el}^b\approx\kappa_{el}^c$. The thermal conductivity is thus the highest along the stacking a direction, whereas the in-plane conductivity is smaller with no noticeable anisotropy between the two in-plane directions b and c. Since Fig. 4 shows that the electrical conductivity of o-$Al_{13}Co_4$ is also the highest along a (appearing in the order $\sigma_a>\sigma_b>\sigma_c$), this material is the best conductor for both the electricity and heat along the stacking a direction perpendicular to the (b,c) atomic planes. The phononic thermal conductivity is shown in the lower panel of Fig. 7. We observe that the anisotropy of κ_{ph} is small and no systematic differences between the three directions can be claimed unambiguously. The anisotropy of the phononic spectrum may therefore not play an important role in the anisotropy of the thermopower presented in Fig. 5.

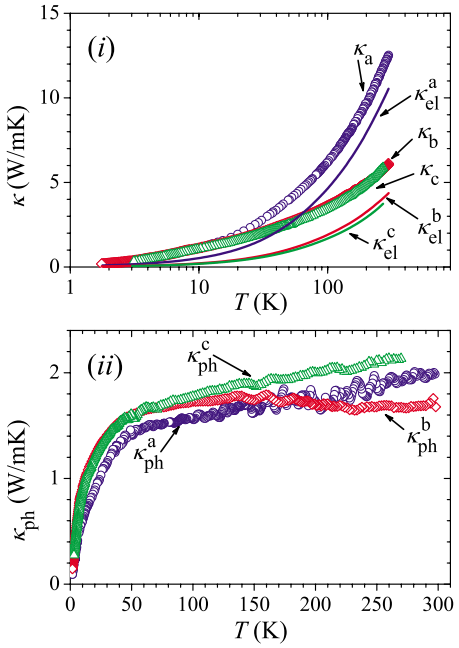

FIG. 7. (Color online) (i) Total thermal conductivity κ of o-$Al_{13}Co_4$ along the three crystallographic directions a, b, and c. Electronic contributions κ_{el}, estimated from the Wiedemann-Franz law, are shown by solid curves. Note the logarithmic temperature scale. (ii) Phononic thermal conductivity $\kappa_{ph}=\kappa-\kappa_{el}$ along the three crystallographic directions.

IV. THEORETICAL *AB INITIO* CALCULATION OF THE TRANSPORT COEFFICIENTS

In an anisotropic crystal, the transport coefficients are generally tensors, depending on the crystallographic direction. For example, the conductivity $\boldsymbol{\sigma}$ (the inverse resistivity $\boldsymbol{\rho}^{-1}$) is a symmetric (and diagonalizable) second-rank tensor, relating the current density $\vec{j}$ to the electric field $\vec{E}$ via the relation $j_i=\Sigma_j\sigma_{ij}E_j$, where $i,j=x,y,z$ denote crystallographic directions. The geometry of our samples (their long axes were along three orthogonal principal directions a, b, and c of the orthorhombic unit cell and the electric field or the temperature gradient were applied along their long axes) imply that diagonal elements of the electrical conductivity, thermoelectric power, and thermal-conductivity tensors were measured in our experiments in a Cartesian x,y,z coordinate system (e.g., the elements $\sigma_{xx}=\sigma_a$, $\sigma_{yy}=\sigma_b$, and $\sigma_{zz}=\sigma_c$ of the conductivity tensor or the elements $S_{xx}=S_a$, $S_{yy}=S_b$, and $S_{zz}=S_c$ of the thermopower tensor were experimentally determined). Since the tensorial ellipsoid exhibits the same symmetry axes as the crystallographic structure, this implies for our orthorhombic o-$Al_{13}Co_4$ crystal that the above tensors are diagonal in the basis of the crystallographic directions a, b, and c. The experimentally determined diagonal elements are thus the only nonzero tensor elements and fully determine the tensors. The Hall coefficient R_H^{ijk} is a third-rank tensor and the geometry of our samples allowed to determine

six tensor elements, comprising all possible orthogonal combinations of the electric current and the magnetic-field directions along the a, b, and c principal axes.

In order to perform quantitative theoretical analysis of the anisotropic transport coefficients, evaluation of the tensor elements requires knowledge of the anisotropic Fermi surface. In the first step, the *ab initio* calculation of the electronic band structure $\varepsilon_{\vec{k},n}$ (where n is the band index) was performed within the framework of the density functional theory (DFT). Calculations were performed for two structural models of the o-$Al_{13}Co_4$ phase, the original model by Grin *et al.*[16] (in the following referred to as the "original" model) and the new version of the model by Grin *et al.*[23] that treats the o-$Al_{13}Co_4$ phase as a cage compound (referred to as the "new" model). In order to test the agreement of the two models with the experiments, the calculations for both models are presented side by side in the following. Here it is worth mentioning that we have taken atomic coordinates of the two models as published in the literature and did not perform additional structural relaxation, in order to see which model, in its present form, conforms better to the experiment. The original model contains no fractionally occupied lattice sites, whereas in the new model, some sites of the original model are split, yielding partial occupation of the sites Al(14) and Al(25)–Al(32) (nine altogether) in the new model with probabilities 0.715, 0.576, 0.516, 0.6, 0.351, 0.554, 0.192, 0.305, and 0.399, respectively. In our calculations, we have selected one possible variant of the unit cell by avoiding too close contacts of the atoms, taking the above occupations as 1, 1, 0.5, 0.5, 0, 1, 0, 0, and 1.

We applied the ABINIT[28] code and the local-density approximation (LDA) (Ref. 29) for the exchange-correlation potential. The electron-ion interactions were described with the norm-conserving pseudopotentials[30] of the Troullier-Martins[31] type. Due to a relatively large number of atoms (102) in the unit cell, the plane-wave cut-off parameter E_{cut} was limited to 220 eV, whereas, according to the tests, $N_{\vec{k}}$=672 $\vec{k}$ points in the full Brillouin zone (BZ) ($N_{\vec{k}}$=96 in the irreducible BZ) were enough to obtain a dense mesh of the energy eigenvalues $\varepsilon_{\vec{k},n}$ required for the calculation of the temperature-dependent transport coefficients, assuring converged results. The *ab initio* calculated Fermi surfaces of the original and the new model, visualized by using the XCRYSDEN program,[32] are presented in Fig. 8. There are eight bands crossing the Fermi energy ε_F, resulting in a significant complexity. It is transparent that the Fermi surface is highly anisotropic, which is at the origin of the experimentally observed anisotropy in the electronic transport coefficients along different crystallographic directions.

In the second step, the temperature-dependent transport coefficients were calculated by means of the Boltzmann semiclassical theory, as implemented in the BOLTZTRAP code.[33] The electrical conductivity tensor $\sigma_{ij}(T,\mu)$, as a function of the temperature T and the chemical potential μ, reads as

$$\sigma_{ij}(T,\mu) = \int \sigma_{ij}(\varepsilon)\left(-\frac{\partial f_\mu(T,\varepsilon)}{\partial \varepsilon}\right)d\varepsilon, \tag{2}$$

where $f_\mu(T,\varepsilon)$ is the Fermi-Dirac distribution. Since $-\partial f_\mu/\partial\varepsilon$ is a narrow bell-like function peaked around ε_F with the width of the order k_BT, this restricts the relevant energies entering Eq. (2) to those in the close vicinity of the Fermi surface. The distribution $\sigma_{ij}(\varepsilon)$ is the sum over the $N_{\vec{k}}$ points $\vec{k}$ and bands n,

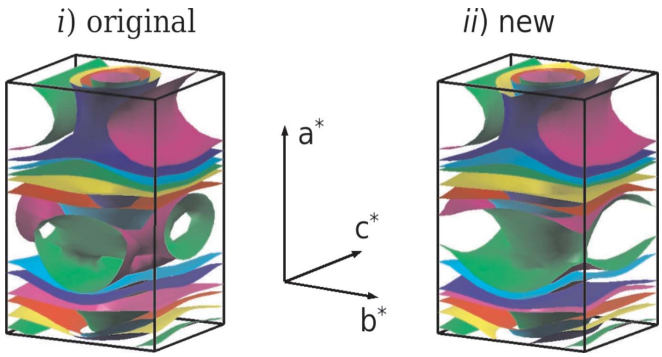

FIG. 8. (Color online) Fermi surface in the first Brillouin zone, calculated *ab initio* for (i) the original o-$Al_{13}Co_4$ model [Grin *et al.* (Ref. 16)] and (ii) the new model [Grin *et al.* (Ref. 23)]. Orientation of the (orthogonal) reciprocal-space axes a^*, b^*, and c^* is also shown.

$$\sigma_{ij}(\varepsilon) = \frac{1}{\Omega}\sum_{\vec{k},n} \sigma_{ij}(\vec{k},n)\,\delta(\varepsilon - \varepsilon_{\vec{k},n}), \tag{3}$$

where Ω is the unit-cell volume. The tensor

$$\sigma_{ij}(\vec{k},n) = \frac{e^2\tau}{\hbar^2}\frac{\partial \varepsilon_{\vec{k},n}}{\partial k_i}\frac{\partial \varepsilon_{\vec{k},n}}{\partial k_j}, \tag{4}$$

where e is the elementary charge, depends on the relaxation time τ. Neglecting its possible dependence on the band index n, τ generally varies with the temperature and crystallographic direction. This variation is not known in our case, so that we are able to present only the product $\rho_{ij}(T,\mu)\tau = \tau/\sigma_{ij}(T,\mu)$. In our calculation, the chemical potential μ equals the Fermi energy, obtained from the *ab initio* calculation. The temperature dependence of the theoretical $\rho_{ij}(T)\tau$ originates from the Fermi-Dirac function.

Similarly, the electronic contribution $\kappa_{\text{el}}^{ij}(T,\mu)$ to the total thermal conductivity κ_{ij} is τ dependent too, and

$$\kappa_{\text{el}}^{ij}(T,\mu) = \frac{1}{e^2T}\int \sigma_{ij}(\varepsilon)(\varepsilon-\mu)^2\left[-\frac{\partial f_\mu(T,\varepsilon)}{\partial\varepsilon}\right]d\varepsilon, \tag{5}$$

so that we are able to present the quantity $\kappa_{\text{el}}^{ij}/\tau$. On the other hand, the relaxation time drops out from the expressions for the Seebeck coefficient $S_{ij}=E_i^{\text{ind}}(\nabla_jT)^{-1}$, where E_i^{ind} is the thermoelectric field in the direction i and ∇_jT is the temperature gradient along j,

$$S_{ij}(T,\mu) = \sum_\alpha (\sigma)^{-1}_{\alpha i}(T,\mu)\frac{1}{eT}\int \sigma_{\alpha j}(\varepsilon)(\varepsilon-\mu) \times\left[-\frac{\partial f_\mu(T,\varepsilon)}{\partial\varepsilon}\right]d\varepsilon, \tag{6}$$

and the Hall coefficient

$$R_H^{ijk}(T,\mu) = \frac{E_j}{j_i B_k} = \sum_{\alpha,\beta} (\sigma)^{-1}_{\alpha j}(T,\mu)\sigma_{\alpha\beta k}(T,\mu)(\sigma)^{-1}_{i\beta}(T,\mu), \tag{7}$$

where $\alpha,\beta=x,y,z$ and

$$\sigma_{\alpha\beta\gamma}(T,\mu) = \int \sigma_{\alpha\beta\gamma}(\varepsilon)\left[-\frac{\partial f_\mu(T,\varepsilon)}{\partial\varepsilon}\right]d\varepsilon. \tag{8}$$

The distribution $\sigma_{\alpha\beta\gamma}(\varepsilon)$ is the sum over the $N_{\vec{k}}$ points $\vec{k}$ and bands n,

$$\sigma_{\alpha\beta\gamma}(\varepsilon) = \frac{1}{\Omega}\sum_{\vec{k},n} \sigma_{\alpha\beta\gamma}(\vec{k},n)\delta(\varepsilon - \varepsilon_{\vec{k},n}), \tag{9}$$

with

$$\sigma_{\alpha\beta\gamma}(\vec{k},n) = \frac{e^3\tau^2}{\hbar^4}\varepsilon_{\gamma\mu\nu}\frac{\partial\varepsilon_{\vec{k},n}}{\partial k_\alpha}\frac{\partial\varepsilon_{\vec{k},n}}{\partial k_\nu}\frac{\partial^2\varepsilon_{\vec{k},n}}{\partial k_\beta\,\partial k_\mu}, \tag{10}$$

where $\varepsilon_{\gamma\mu\nu}$ denotes the Levi-Civita tensor.[34,35] Therefore, since the dependence of the relaxation time τ on the temperature and the crystallographic direction is not known, we are able to present the *ab initio* calculated products $\rho_{ij}(T)\tau$ and $\kappa_{\rm el}^{ij}(T)/\tau$, whereas $S_{ij}(T)$ and $R_H^{ijk}(T)$ can be calculated directly in absolute figures. In the following, these coefficients are presented for the original and the new model and a comparison to the experiments is made. It is also worth mentioning that the electrical resistivity ρ_{ij} and the electronic thermal conductivity $\kappa_{\rm el}^{ij}$ do not distinguish between the negative electron-type carriers and the positive hole-type carriers (the elementary charge appears in their expressions as e^2 and hence does not distinguish between the electrons $(-e)$ and holes $(+e)$, whereas the thermopower S_{ij} and the Hall coefficient R_H^{ijk} distinguish between the electrons and holes (the charge in their expressions appears as e or $1/e$, respectively, hence distinguishing its sign).

A. Electrical resistivity

The calculated $\rho_a\tau$, $\rho_b\tau$, and $\rho_c\tau$ are displayed in Fig. 9(i) for the original model and in Fig. 9(ii) for the new model. In comparison to the experimental resistivity (Fig. 4), both models correctly reproduce the order of the anisotropic resistivity in a qualitative manner (the theoretical $\rho_a\tau<\rho_b\tau<\rho_c\tau$ agrees with the experimental $\rho_a<\rho_b<\rho_c$). The new model reproduces slightly better the experimental fact that the anisotropy between the two in-plane resistivities ρ_b and ρ_c is small. In the approximation of a direction independent τ (so that τ drops out of the resistivity ratios), we obtain the theoretical ratios at $T=300$ K for the original model $\rho_c/\rho_b=1.6$, $\rho_c/\rho_a=7.7$, and $\rho_b/\rho_a=4.8$, whereas the ratios for the new model are $\rho_c/\rho_b=1.4$, $\rho_c/\rho_a=5.4$, and $\rho_b/\rho_a=3.8$. Comparing to the experimental 300 K ratios $\rho_c/\rho_b=1.07$, $\rho_c/\rho_a=2.6$, and $\rho_b/\rho_a=2.5$, we see that the new model gives considerably better agreement to the experiment, though the agreement is still qualitative only.

B. Electronic thermal conductivity

The theoretical $\kappa_{\rm el}^a/\tau$, $\kappa_{\rm el}^b/\tau$, and $\kappa_{\rm el}^c/\tau$ are displayed in Fig. 10(i) for the original model and in Fig. 10(ii) for the new model. In comparison to the experimental electronic thermal conductivity [solid lines in Fig. 7(i)], both models correctly reproduce the order of the anisotropic $\kappa_{\rm el}$ in a qualitative manner (the theoretical $\kappa_{\rm el}^a/\tau>\kappa_{\rm el}^b/\tau>\kappa_{\rm el}^c/\tau$ agrees with the experimental $\kappa_{\rm el}^a>\kappa_{\rm el}^b>\kappa_{\rm el}^c$). Both models also reproduce the experimental fact that the anisotropy between the two in-plane conductivities $\kappa_{\rm el}^b$ and $\kappa_{\rm el}^c$ is small. In the approximation of a direction independent τ, we obtain the theoretical ratios at $T=300$ K for the original model $\kappa_{\rm el}^a/\kappa_{\rm el}^b=4.7$, $\kappa_{\rm el}^a/\kappa_{\rm el}^c=7.6$, and $\kappa_{\rm el}^b/\kappa_{\rm el}^c=1.6$, whereas the ratios for the new model are $\kappa_{\rm el}^a/\kappa_{\rm el}^b=3.7$, $\kappa_{\rm el}^a/\kappa_{\rm el}^c=5.5$, and $\kappa_{\rm el}^b/\kappa_{\rm el}^c=1.5$. Comparing to the experimental 300 K ratios $\kappa_{\rm el}^a/\kappa_{\rm el}^b=2.3$, $\kappa_{\rm el}^a/\kappa_{\rm el}^c=2.5$, and $\kappa_{\rm el}^b/\kappa_{\rm el}^c=1.07$, we see that the new model gives better agreement to the experiment, though the agreement is still qualitative only. One reason for the qualitative level of agreement between the theory and experiment is also the fact that the experimental $\kappa_{\rm el}^{ii}$ coefficients were derived from the total thermal conductivity κ^{ii} by using the Wiedemann-Franz law, which is by itself an approximation to the true $\kappa_{\rm el}^{ii}$.

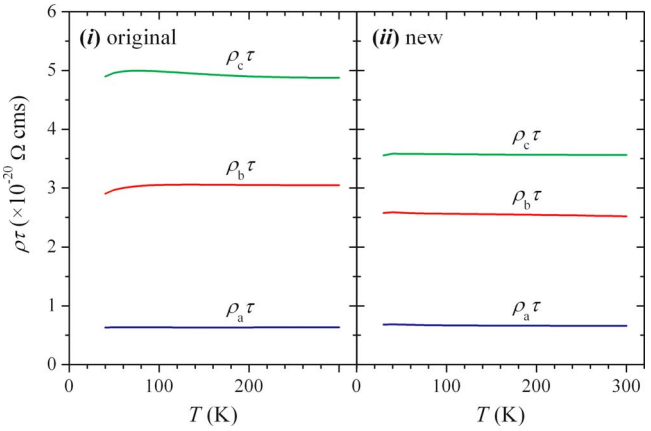

FIG. 9. (Color online) Theoretical anisotropic $\rho_a\tau$, $\rho_b\tau$, and $\rho_c\tau$ (products of the electrical resistivity and the relaxation time), calculated *ab initio* for (i) the original *o*-$Al_{13}Co_4$ model [Grin *et al.* (Ref. 16)] and (ii) the new model [Grin *et al.* (Ref. 23)].

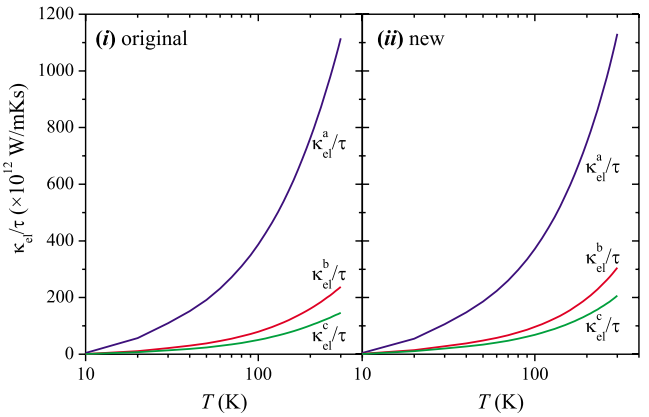

FIG. 10. (Color online) Theoretical anisotropic $\kappa_{\rm el}^a/\tau$, $\kappa_{\rm el}^b/\tau$, and $\kappa_{\rm el}^c/\tau$ (electronic thermal conductivities divided by the relaxation time), calculated *ab initio* for (i) the original *o*-$Al_{13}Co_4$ model [Grin *et al.* (Ref. 16)] and (ii) the new model [Grin *et al.* (Ref. 23)].

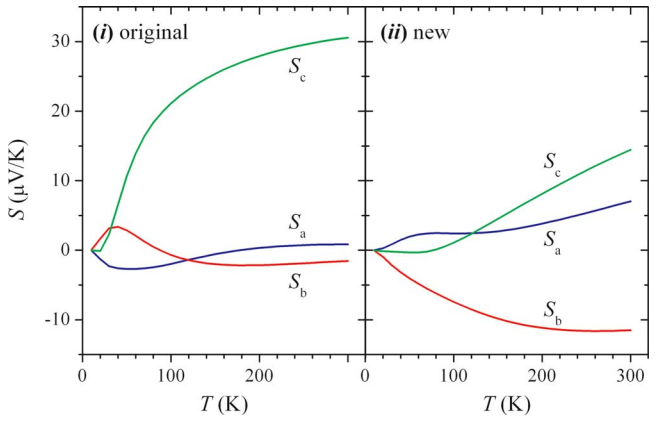

FIG. 11. (Color online) Theoretical anisotropic thermopowers S_a, S_b, and S_c, calculated *ab initio* for (i) the original *o*-$Al_{13}Co_4$ model [Grin *et al.* (Ref. 16)] and (ii) the new model [Grin *et al.* (Ref. 23)].

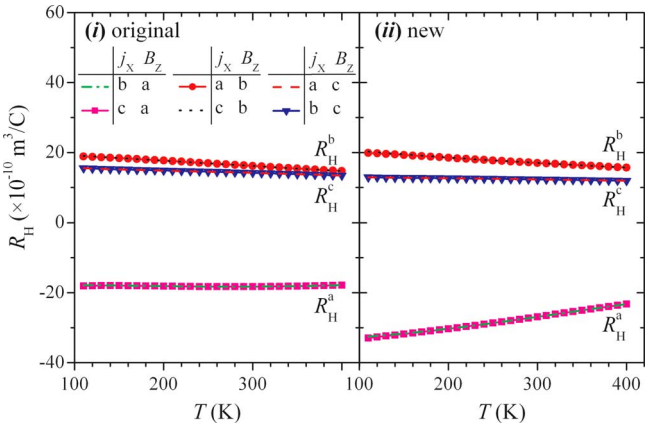

FIG. 12. (Color online) Theoretical anisotropic Hall coefficient, calculated *ab initio* for (i) the original *o*-$Al_{13}Co_4$ model [Grin *et al.* (Ref. 16)] and (ii) the new model [Grin *et al.* (Ref. 23)]. R_H was calculated for the same set of current and field directions as employed in the experimental measurements of the Hall coefficient shown in Fig. 6. The superscript *a*, *b*, or *c* on R_H denotes the direction of the magnetic field. There are three groups of curves, each consisting of two practically indistinguishable curves (see text).

C. Thermoelectric power

Since the relaxation time τ drops out of the expression for S_{ij}, this coefficient can be calculated in absolute figures and hence provides better test for comparison to the experiment. The theoretical S_a, S_b, and S_c are displayed in Fig. 11(i) for the original model and in Fig. 11(ii) for the new model. Comparing to the experimental thermopower of Fig. 5, where the anisotropic thermopowers appear in the order $S_a > S_c > S_b$, we observe that the original model fails completely in both the order of the thermopowers and their values. The new model is slightly better; it gives a relatively good agreement of the theoretical S_b to the experiment in both its temperature dependence and the magnitude (the theoretical 300 K value $S_b = -12$ μV/K compares reasonably to the experimental $S_b = -17$ μV/K), whereas the theoretical S_a and S_c do not match the corresponding experimental parameters. At temperatures below 120 K, the order of the theoretical thermopowers of the new model $S_a > S_c > S_b$ still agrees with the experimental one. However, the theoretical S_a and S_c cross each other at 120 K giving an incorrect order at higher temperatures. The new model thus gives a qualitative agreement to the experiment at temperatures below 120 K, whereas at higher temperatures, only S_b remains in qualitative agreement to the experiment. The fact that the sign of the thermopower changes with the crystallographic directions is also reproduced theoretically (at temperatures below 120 K, the theoretical $S_a > 0$, $S_c \approx 0$, and $S_b < 0$ of the new model match correctly the experiment).

D. Hall coefficient

The Hall coefficient R_H^{ijk} can also be calculated in absolute figures. The theoretical anisotropic Hall coefficient, calculated for the same set of combinations of the current and field directions as the experimental one in Fig. 6, is shown in Fig. 12(i) for the original model and in Fig. 12(ii) for the new model. Both models correctly reproduce the experimental fact that the six theoretical R_H^{ijk} data sets form three groups of two R_H^{ijk} curves, where the magnetic field in a given crystallographic direction yields the same value of the Hall coefficient for the current along the other two crystallographic directions in the perpendicular plane. Both models also correctly reproduce the order of appearance of the anisotropic Hall coefficient (the theoretical order $R_H^b > R_H^c > R_H^a$ matches the experimental one from Fig. 6) and the crystallographic-direction-dependent change of sign $R_H^b > 0$ and $R_H^a < 0$. The R_H^c coefficient, the value of which is intermediate to R_H^b and R_H^a, is theoretically less well reproduced. Experimentally we have $R_H^c \approx 0$ (even slightly negative), whereas both models yield theoretically $R_H^c > 0$. The theoretical R_H^c value of the new model is, however, smaller (closer to zero) than R_H^c of the original model, thus conforming better to the experiment at a qualitative level. At a quantitative level, none of the two models reproduces the experimental figures, giving too large values for all combinations of directions. The original and the new model thus give qualitative agreement to the experimental anisotropic Hall coefficient but both fail quantitatively to a similar extent.

V. SUMMARY AND DISCUSSION

We have investigated magnetic susceptibility, electrical resistivity, thermoelectric power, Hall coefficient, and thermal conductivity of the orthorhombic *o*-$Al_{13}Co_4$ complex metallic compound, belonging to the $Al_{13}TM_4$ group of decagonal approximants with four atomic layers within one periodic unit of ≈ 0.8 nm along the stacking *a* direction and comprising 102 atoms in the giant unit cell. Our main objective was to determine the crystallographic-direction-dependent anisotropy of the investigated physical parameters when measured within the (b,c) atomic planes, corresponding to the quasiperiodic planes in the related *d*-QCs, and along the stacking *a* direction perpendicular to the planes,

corresponding to the periodic direction in *d*-QCs. Magnetic susceptibility shows considerable anisotropy, appearing in the order $\chi_a < \chi_b < \chi_c$. The in-plane anisotropy is weak, whereas the anisotropy between the in-plane directions and the stacking *a* direction is stronger. The linear positive paramagnetic $M(H)$ relation suggests that the susceptibility is predominantly determined by the Pauli-spin paramagnetism of conduction electrons.

Electrical resistivity of *o*-$Al_{13}Co_4$ is relatively low in all crystallographic directions, with the RT values in the range 69–180 $\mu\Omega$ cm. There exists significant anisotropy between the in-plane resistivity and the resistivity along the stacking *a* direction by a factor about 2.5, whereas the anisotropy between the two in-plane directions *b* and *c* is much smaller. The anisotropic resistivity appears in the order $\rho_a < \rho_b < \rho_c$ (even the inequality $\rho_a \ll \rho_b < \rho_c$ may be considered to hold), so that the stacking *a* direction is the most electrically conducting one. The PTC of the resistivity in all crystallographic directions reveals that the electron-phonon interaction provides an important scattering mechanism.

The anisotropic thermopower of *o*-$Al_{13}Co_4$ appears in the order $S_a > S_c > S_b$ and exhibits a change of sign along different crystallographic directions. It is positive along the stacking *a* direction ($S_a > 0$), almost symmetrically negative for the in-plane *b* direction ($S_b < 0$) and close to zero for the second in-plane *c* direction ($S_c \approx 0$). While S_a and S_b exhibit relatively strong temperature dependence, S_c shows almost no temperature dependence in the investigated temperature range. The observed anisotropy of the thermopower, ranging between positive and negative values, suggests that the Fermi surface consists of electronlike and holelike parts, which compensate each other for some crystallographic directions to yield a thermopower close to zero.

The Hall coefficient R_H of *o*-$Al_{13}Co_4$ exhibits pronounced anisotropy, where the magnetic field in a given crystallographic direction yields practically the same R_H for the current along the other two crystallographic directions in the perpendicular plane. The anisotropic Hall coefficient appears in the order $R_H^b > R_H^c > R_H^a$ and exhibits a change of sign with the direction of the magnetic field, reflecting complicated structure of the Fermi surface that consists of electronlike and holelike parts. The negative $R_H^a < 0$ is electronlike for the magnetic field along the stacking *a* direction, whereas the positive $R_H^b > 0$ behaves holelike for the field along the in-plane *b* direction. For the field along the second in-plane direction *c*, $R_H^c \approx 0$ suggests that the electronlike and holelike contributions are of comparable importance.

The anisotropic thermal conductivity of *o*-$Al_{13}Co_4$ appears in the order $\kappa^a > \kappa^b \approx \kappa^c$, and the same order applies to the electronic part, $\kappa_{\mathrm{el}}^a > \kappa_{\mathrm{el}}^b \approx \kappa_{\mathrm{el}}^c$. Thermal conductivity is the highest along the stacking *a* direction, whereas the in-plane conductivity is smaller with no noticeable anisotropy between the *b* and *c* directions. Since the electrical conductivity of *o*-$Al_{13}Co_4$ is also the highest along *a*, this material is the best conductor for both the electricity and heat along the stacking *a* direction perpendicular to the (b,c) atomic planes. Electrons (and holes) are majority heat carriers at RT along all three crystallographic directions.

In an attempt to perform quantitative theoretical analysis of the anisotropic transport coefficients, the anisotropic Fermi surface was calculated *ab initio* for the two structural models of the *o*-$Al_{13}Co_4$ phase, the original model by Grin *et al.*[16] and the new version of the model by Grin *et al.*[23] that treats the *o*-$Al_{13}Co_4$ phase as a cage compound. The atomic coordinates of the two models were taken as published in the literature and no additional structural relaxation was performed in order to see which model, in its present form, conforms better to the experiment. Using the theoretical Fermi surface, the transport coefficients were calculated *ab initio* by means of the Boltzmann semiclassical theory. The aim of the calculations was to check whether the strong anisotropies in the transport coefficients can be ascribed to the electronic structure of the *o*-$Al_{13}Co_4$ phase, whereas no attempt was made to reproduce their temperature dependence. Since the dependence of the relaxation time τ on the temperature and the crystallographic direction was not known, we were able to analyze the *ab initio* calculated products $\rho_{ij}(T)\tau$ and $\kappa_{\mathrm{el}}^{ij}(T)/\tau$, whereas $S_{ij}(T)$ and $R_H^{ijk}(T)$ were calculated directly in absolute figures. While the electrical resistivity ρ_{ij} and the electronic thermal conductivity $\kappa_{\mathrm{el}}^{ij}$ do not distinguish between the negative electron-type and positive hole-type carriers, the thermopower S_{ij} and the Hall coefficient R_H^{ijk} distinguish between the electrons and holes.

Both models correctly reproduce the anisotropy of the electrical resistivity and the electronic thermal conductivity at a qualitative level. The new model reproduces considerably better the 300 K ρ_{ii}/ρ_{jj} and $\kappa_{\mathrm{el}}^{ii}/\kappa_{\mathrm{el}}^{jj}$ ratios along different crystallographic directions and the experimental fact that the in-plane anisotropy of these two transport coefficients is small, though the agreement is still qualitative only.

Regarding the anisotropic thermopower, the original model fails completely in both the order of appearance of the thermopowers and their values. The new model is slightly better but still qualitative only. It gives a relatively good agreement of the theoretical S_b to the experiment in both its temperature dependence and the magnitude, whereas the theoretical S_a and S_c do not match the corresponding experimental parameters. The order of the anisotropic theoretical thermopowers of the new model agrees with the experimental one in the low-temperature regime below 120 K. The new model also correctly reproduces the fact that the thermopower changes sign with the crystallographic direction.

Both models also correctly reproduce the anisotropy of the Hall coefficient and the experimental fact that the magnetic field in a given crystallographic direction yields the same value of the Hall coefficient for the current along the other two orthogonal directions in the perpendicular plane. The crystallographic-direction-dependent change of sign $R_H^b > 0$ and $R_H^a < 0$ is also well reproduced theoretically, whereas the R_H^c coefficient, the value of which is intermediate to R_H^b and R_H^a, is less well reproduced. Experimentally, $R_H^c \approx 0$ (even slightly negative), whereas both models yield theoretically $R_H^c > 0$. The theoretical R_H^c value of the new model is, however, smaller (closer to zero) than R_H^c of the original model, thus conforming better to the experiment at a qualitative level. At a quantitative level, none of the two models reproduces the experimental figures, giving too large values for all combinations of the current and field directions. The original and the new model thus give qualitative agreement to the experimental anisotropic Hall coefficient but both fail quantitatively to a similar extent.

Structural relaxation of the two models of o-$Al_{13}Co_4$ could yield better agreement to the experiment. In its present form, the new Grin *et al.* model[23] conforms better to the experiment and can be considered superior to the original one.[16]

The lack of quantitative agreement between the *ab initio*-calculated theoretical transport coefficients and the experiments could indicate limited applicability of the Boltzmann semiclassical transport theory to the complex electronic structure of the o-$Al_{13}Co_4$ giant-unit-cell intermetallic. The Boltzmann theory is based on the concept of a charge-carrier wave packet propagating at a velocity $\vec{v}_{\vec{k},n}=(1/\hbar)\partial\varepsilon_{\vec{k},n}/\partial\vec{k}$. The validity of the wave packet concept requires the condition that the extension L_{wp} of the wave packet of the charge carrier is smaller than the distance $\lambda=v\tau$ of traveling between two scattering events separated by a time τ (the so-called ballistic propagation). On the contrary, when $\lambda<L_{\mathrm{wp}}$, a condition that can be realized for sufficiently slow charge carriers, the propagation is nonballistic and the semiclassical model breaks down. Small velocities are found in systems with weak band dispersion, i.e., when the derivatives $\partial\varepsilon_{\vec{k},n}/\partial\vec{k}$ are small. The electrical resistivity of slow charge carriers has been elaborated theoretically by Trambly de Laissardière *et al.*,[36] whereas the application of this theory to the complex intermetallic compounds can be found in our papers on the resistivity of the $Al_4(Cr,Fe)$ decagonal approximant.[13,14] Upon increased scattering by quenched defects and/or temperature effects (electron-phonon scattering), the theory predicts a transition from the Boltzmann-type PTC resistivity to the non-Boltzmann-type NTC resistivity. For a moderate concentration of quenched defects, the temperature-dependent resistivity exhibits a maximum at the transition from the low-temperature PTC resistivity to the NTC resistivity at elevated temperatures. The PTC resistivity of o-$Al_{13}Co_4$ (Fig. 4) indicates that this system is in the Boltzmann regime and the condition $\lambda>L_{\mathrm{wp}}$ is satisfied. However, the relatively weak PTC for all three crystallographic directions suggests that the velocity of charge carriers may already be slow enough that the non-Boltzmann contribution to the resistivity starts to be non-negligible.

The relatively large residual resistivity upon $T\rightarrow 0$ (anisotropic $\rho^{2\ \mathrm{K}}$ values in the range 47–129 $\mu\Omega$ cm) indicates the presence of quenched disorder in the samples. Since Fig. 1 shows that the samples are free of secondary phases and grain boundaries, this disorder is very likely the chemical and geometric disorder arising from partially occupied lattice sites, as incorporated in the new Grin *et al.*[23] model. The original Grin *et al.*[16] model contains no partially occupied sites, so that this kind of disorder should be largely absent and the residual resistivity should become small. The large residual resistivity is another fact in favor of the new model. This is further supported by the anisotropy of the residual resistivity along the three crystallographic directions. The residual resistivity arises from elastic scattering of electrons on quenched defects. Assuming the defects are due to partial occupation of the lattice sites (hence being an intrinsic feature of the o-$Al_{13}Co_4$ structure), their concentration is different along different crystallographic directions, and the mean-free path λ between scattering events is anisotropic. Consequently, the residual resistivity becomes anisotropic, too.

ACKNOWLEDGMENTS

This work was done within the activities of the Sixth Framework EU Network of Excellence "Complex Metallic Alloys" (Contract No. NMP3-CT-2005-500140). A.S. acknowledges support of the Ministry of Science, Education and Sports of the Republic of Croatia through Research Project No. 035-0352826-2848.

[1] T. Shibuya, T. Hashimoto, and S. Takeuchi, J. Phys. Soc. Jpn. **59**, 1917 (1990).
[2] S. Martin, A. F. Hebard, A. R. Kortan, and F. A. Thiel, Phys. Rev. Lett. **67**, 719 (1991).
[3] Wang Yun-ping and Zhang Dian-lin, Phys. Rev. B **49**, 13204 (1994).
[4] Lin Shu-yuan, Wang Xue-mei, Lu Li, Zhang Dian-lin, L. X. He, and K. H. Kuo, Phys. Rev. B **41**, 9625 (1990).
[5] Zhang Dian-lin, Lu Li, Wang Xue-mei, Lin Shu-yuan, L. X. He, and K. H. Kuo, Phys. Rev. B **41**, 8557 (1990).
[6] Wang Yun-ping, Zhang Dian-lin, and L. F. Chen, Phys. Rev. B **48**, 10542 (1993).
[7] Zhang Dian-lin, Cao Shao-chun, Wang Yun-ping, Lu Li, Wang Xue-mei, X. L. Ma, and K. H. Kuo, Phys. Rev. Lett. **66**, 2778 (1991).
[8] K. Edagawa, M. A. Chernikov, A. D. Bianchi, E. Felder, U. Gubler, and H. R. Ott, Phys. Rev. Lett. **77**, 1071 (1996).
[9] D. N. Basov, T. Timusk, F. Barakat, J. Greedan, and B. Grushko, Phys. Rev. Lett. **72**, 1937 (1994).
[10] M. Krajčí and J. Hafner, Phys. Rev. B **58**, 5378 (1998).
[11] G. Trambly de Laissardière and T. Fujiwara, Phys. Rev. B **50**, 9843 (1994).
[12] A. Smontara, I. Smiljanić, J. Ivkov, D. Stanić, O. S. Barišić, Z. Jagličić, P. Gille, M. Komelj, P. Jeglič, M. Bobnar, and J. Dolinšek, Phys. Rev. B **78**, 104204 (2008).
[13] J. Dolinšek, P. Jeglič, M. Komelj, S. Vrtnik, A. Smontara, I. Smiljanić, A. Bilušić, J. Ivkov, D. Stanić, E. S. Zijlstra, B. Bauer, and P. Gille, Phys. Rev. B **76**, 174207 (2007).
[14] J. Dolinšek, S. Vrtnik, A. Smontara, M. Jagodič, Z. Jagličić, B. Bauer, and P. Gille, Philos. Mag. **88**, 2145 (2008).
[15] D. W. Deng, Z. M. Mo, and K. H. Kuo, J. Phys.: Condens. Matter **16**, 2283 (2004).
[16] J. Grin, U. Burkhardt, M. Ellner, and K. Peters, J. Alloys Compd. **206**, 243 (1994).
[17] R. C. Hudd and W. H. Taylor, Acta Crystallogr. **15**, 441 (1962).
[18] J. Grin, U. Burkhardt, M. Ellner, and K. Peters, Z. Kristallogr. **209**, 479 (1994).
[19] B. Zhang, V. Gramlich, and W. Steurer, Z. Kristallogr. **210**, 498 (1995).
[20] L.-E. Edshammar, Acta Chem. Scand. (1947-1973) **18**, 2294

(1964).
[21] L.-E. Edshammar, Acta Chem. Scand. (1947-1973) **19**, 2124 (1965).
[22] Z. A. Chaudhury and C. Suryanarayana, J. Less-Common Met. **91**, 181 (1983).
[23] Yu. Grin, B. Bauer, U. Burkhardt, R. Cardoso-Gil, J. Dolinšek, M. Feuerbacher, P. Gille, F. Haarmann, M. Heggen, P. Jeglič, M. Müller, S. Paschen, W. Schnelle, and S. Vrtnik, EUROMAT 2007: European Congress on Advanced Materials and Processes, Nürnberg, Germany, 2007 (unpublished), Book of Abstracts, p. 30.
[24] P. Gille and B. Bauer, Cryst. Res. Technol. **43**, 1161 (2008).
[25] P. W. Selwood, *Magnetochemistry* (Interscience, New York, 1956), p. 78.
[26] Y. Yamada, Y. Yokoyama, K. Matono, and K. Fukaura, Jpn. J. Appl. Phys., Part 1 **38**, 52 (1999).
[27] J. T. Markert, J. L. Cobb, W. D. Bruton, A. K. Bhatnagar, D. G. Naugle, and A. R. Kortan, J. Appl. Phys. **76**, 6110 (1994).
[28] X. Gonze *et al.*, Comput. Mater. Sci. **25**, 478 (2002); The ABINIT computer program is a common project of the Université Catholique de Louvain, Corning Incorporated, and other contributors (http://www.abinit.org).
[29] J. P. Perdew and Y. Wang, Phys. Rev. B **45**, 13244 (1992).
[30] M. Fuchs and M. Scheffler, Comput. Phys. Commun. **119**, 67 (1999).
[31] N. Troullier and J. L. Martins, Phys. Rev. B **43**, 1993 (1991).
[32] A. Kokalj, Comput. Mater. Sci. **28**, 155 (2003); code available from http://www. xcrysden.org
[33] G. K. H. Madsen and J. Singh, Comput. Phys. Commun. **175**, 67 (2006).
[34] C. M. Hurd, *The Hall Effect in Metals and Alloys* (Plenum, New York, 1972).
[35] H. J. Weber, *Essential Mathematical Methods for Physicists* (Elsevier Academic, San Diego, USA, 2004).
[36] G. Trambly de Laissardière, J.-P. Julien, and D. Mayou, Phys. Rev. Lett. **97**, 026601 (2006).